Experimental validation of a simple dynamic model of a laboratory scale recirculating aquaculture system fitted with submerged membrane bioreactor

Guilherme Araujo Pimentel, Pedro Miranda Almeida, Anne-Lise Hantson, Alain Rapaport, Alain Vande Wouwer

Experimental validation of a simple dynamic model of a laboratory scale recirculating aquaculture system fitted with a submerged membrane bioreactor

Guilherme A. Pimentel[a,b,c,e], Pedro Almeida[b], Anne-Lise Hantson[d], Alain Rapaport[c,e], Alain Vande Wouwer[b]

[a] *Department of Automation and Energy, Universidade Federal do Rio Grande do Sul, Av. Osvaldo Aranha, 103, Porto Alegre, RS, Brazil*
[b] *University of Mons - Automatic Control Laboratory - Biosys, Boulevard Dolez 31, 7000 Mons, Belgium*
[c] *Equipe Projet INRA-INRIA MODEMIC, Route des Lucioles 06902 Sophia-Antipolis, France*
[d] *Service de Chimie et Biochimie Appliquées, Université de Mons, 56 Rue de l'épargne,B-7000 Mons, Belgium*
[e] *UMR INRA-SupAgro MISTEA, 2 Place Viala 34060 Montpellier, France*

Abstract

Submerged membrane bioreactors (sMBR's) are a promising technology for nitrogen removal in recirculating aquaculture systems (RAS's). However, there are still relatively few reports on the experimental application of this strategy. In this study, a laboratory-scale system, mimicking a RAS fitted with a sMBR, was designed and automated, and a simple dynamic sMBR model including biological and physical phenomena was validated. The system was analyzed based on measurements collected by a data logging structure involving a programmable logic controller (PLC), an industrial network protocol and a LabView application software. This study confirms the suitability of sMBR systems within aquaculture applications. The dynamic model has good predictive capabilities and could be used for the design of advanced control structures, such as model predictive control.

Keywords: Recirculating aquaculture system; Laboratory-Scale System;

Email addresses: guilherme.pimentel@ufrgs.br (Guilherme A. Pimentel), pedro.almeida@umons.ac.be (Pedro Almeida), anne-lise.hantson@umons.ac.be (Anne-Lise Hantson), rapaport@supagro.inra.fr (Alain Rapaport), alain.vandewouwer@umons.ac.be (Alain Vande Wouwer)

Waste-Water Treatment; Membrane Bioreactors; Dynamic Modeling; Control;

1. Introduction

The growth of the world population and the scarcity of water, land and other natural resources motivate the use of recirculating aquaculture systems and their optimization [1]. For most agro-food processes, profits are computed based on the quantity of consumed resources, production yield by process footprint, and environmental impact. Especially in aquaculture systems, the ratio between fresh incoming water and recirculated water is a determining economic and ecological factor, usually set to a maximum of 10% of the total volume replaced per day [2]. However, if the recirculated water is not properly treated, harmful compounds could accumulate, such as ammonia and nitrate. In order to prevent this accumulation, the use of rotating disk contactors, trickling filters, bead filters or fluidized sand biofilters [3] is a common solution. On the other hand, submerged membrane bioreactors (sMBR's) have been increasingly used in water treatment. They accomplish the combined functions of an aerobic activated sludge system, a secondary clarifier, and a tertiary filter [4], reducing the process footprint and producing high-quality effluent [5, 6, 7, 8]. Despite these decisive advantages, only a limited number of applications have been reported in recirculating systems [9]. One of the reasons is the fouling of the membrane, which decreases membrane permeability, such that the membrane requires periodic cleaning [10].

The use of submerged membrane bioreactors (sMBR's) in recirculating aquaculture systems (RAS's) is therefore relatively new. The RAS differs from conventional domestic and industrial wastewater treatment in the composition of the inflow and specially in the low total suspended solids (TSS) concentration [11]. These aspects contribute to different rates of fouling and internal recirculation flows, which affect the operating and cleaning cycles of sMBR's as well as the membrane cleaning procedures. Also, [12, 13] evidenced a remarkable reduction in wastewater and residue load in RAS treatment when compared to

conventional water treatment in aquaculture systems.

As experimental data from aquaculture systems with sMBR is scarce, it is of interest to develop additional laboratory-scale studies, and the objective of this work is threefold: The first objective is to set-up a laboratory-scale RAS and collect informative experimental data. Indeed, industrial processes should not be disturbed so as to avoid any harmful effect on the fish population, and a laboratory-scale platform with synthetic wastewater is ideal for developing experimental analysis and model validation, with data covering a range of operating conditions. This paper gives a full description of a suitable laboratory-scale process; The second objective is to validate experimentally a dynamic model that was recently proposed and analyzed by the authors in [14]. The model is four-dimensional and possesses ten parameters to be identified. In view of its modest size, this model is a good basis to implement model-based optimization and control; The third objective is to propose a dedicated parameter identification procedure that exploits the characteristics of the dynamic model and the existence of three different time-scales. This procedure allows the identification of the model parameters from data collected at laboratory scale, with satisfactory accuracy and precision, and could be used in practice for setting-up models of full-scale plants.

This paper is organized as follows. Section 2 describes the laboratory-scale process, including sensors and actuators, as well as the data acquisition system. Section 3 briefly presents a simple mathematical model proposed in [14, 15], together with a parameter identification strategy. The main experimental results are then presented in Section 4 and discussed in Section 5. Finally, some conclusions are drawn in Section 6.

2. Materials and Methods

2.1. Process Description

Recirculating aquaculture systems are sustainable fish production facilities in terms of water usage. Water reuse is possible only if efficient nitrification,

denitrification and removal of organic matter are achieved. A sMBR can be incorporated into the system in view of its high effluent quality. In this study, we undertake a case study involving the production of tilapia and trout, which are susceptible to high concentrations of ammonia resulting from fish feces and excretion, but are tolerant to nitrate [16]. Future studies could be carried out with other species, where the nitrate concentration plays a critical role in the process.

2.2. Experimental Setup

The laboratory-scale RAS-sMBR is designed to remove nitrogen and solid matter (see Figure 1). The influent is composed of a synthetic wastewater that mimics fish excrement with ammonia mass flow of around 19.8 mg/h. This value is based on the ammonia excretion values reported by [17] and [18], for a total fish basin volume of 0.05 m^3 and a fish density of 24 kg/m^3.

The bioreactors have a total volume of 0.22 m^3 divided into an anaerobic compartment (41% of the total volume), an aerobic compartment (41%), and a compartment with submerged microfiltration membranes (18%). The recirculation between the sMBR and the nitrification tank is 0.7 m^3/d while the recirculation between the nitrification and denitrification tanks is 0.7 m^3/d. The total area of the membrane is 0.35 m^2 (Microdyn-Nadir Gmbh), working at $t_{permeate} = 0.0035$ d (i.e., 5 min) filtration and $t_{relax} = 6.94 \times 10^{-4}$ d (i.e., 1 min) relaxation. The permeate production is around 18.7 $L/m^2/h$, and membrane aeration is around 20 m^3/d. The suspended solids concentration in the membrane compartment ranges from 0.05 to 0.6 g/L. Online data, including temperature, flows and trans-membrane pressure (TMP), are measured every second. Offline measurements of suspended solids concentration, pH, air-flow rates and ammonium concentration are carried out daily. The measurement of ammonia concentration is carried out using HACH kits $LCK - 304$. The confidence interval at 95 % is $\pm$ 0.012 mg/L. Note that ammonia can be presented in water in two forms, which depends on the pH of the water. When pH is less then 7 the ammonia is mainly presented as its ionized form (NH_4^+), as pH

increases above 7 its un-ionized (NH_3) form is also present.

The system includes five pumps of three different types. The intermediate circulation pumps (MP1, MP2, MP3) are magnetic couple AC pumps (IWAKI model MD-6-230GS01), which allow flows up to 8 L/min. The global recirculation and backwash pump is a diaphragm 24 Vdc pump (SHURflo model 8000-991-236) with a maximum flow rate of 2 L/min. The last pump is the dosing pump (ISMATEC model Reglo Digital MS-2/6-160), whose flow is adjusted to emulate the effect of fish excretion by injecting a solution containing ammonia into the system.

The AC pump sources are phase-angle dimmers (NS−80 from FG ELEKTRONIK) that allow the PLC to control the pumps through its analog outputs. The diaphragm pump is a DC pump powered by a DC driver, which allows the PLC to change the flow using pulse width modulation (PWM).

To control the pump flow rates, the levels of the tanks and the differential pressure across the membrane, the following sensors are used: level sensors, which consist of a simple float switch that prevents the tank from overflowing; flow-meters, ranging from 0.05 to 10 L/min, which allow a large range of operating conditions, and a pressure sensor that is used for the TMP measurement and ranges from -1 to 1.6 bar, producing an output current of 4 to 20 mA.

Two motorized 3-way valves (V1 and V2) are used to reverse the flow from permeate to backwash on the sMBR module and V3 controls the waste flow. The system uses reinforced flexible tubing of 13 mm in diameter.

For the aeration of the nitrification tank, a Roeflex disc diffuser from *Passavant − Geiger Gmbh* is used, which permits good diffusion of air at the bottom of the tank. The air source for the nitrification tank is separate from the sMBR air source. For the nitrification tank, an air pump with variable air flow is used while constant flow is applied to the sMBR. Airflow sensors and manual control allow manipulation of the airflow rate in a range from 0 to 300 NL/h (NL are normal liters, referring to 0 ℃ and 1 atm).

The membrane used is a BIO-CEL Lab from Microdyn-Nadir Gmbh. It has a membrane surface area of 0.35 m^2 and is installed in a PVC frame with

integrated cross-flow aeration via a membrane diffuser. Connections for permeate drainage and air supply are already provided. The Nadir membrane (type UP150) has 150 MWCO (Molecular weight cut-off) [kDa], and is made of Polyethersulfone (PES). The material is hydrophilic with a high chemical resistance (pH from 0 to 14 and max temperature 95 ℃). The membrane has been designed for environmental protection, metal processing, textiles, paper, food/dairy, pharma/biotech and chemical processes. The membrane is identical to that of the full-scale BIO-CEL module, making the laboratory-scale device representative of a real-life process [19].

For data acquisition and control, a PLC S7-1200 from Siemens is used, which has all the inputs and outputs needed for the process monitoring and control. To complete the monitoring part, a PC is used as an industrial network using OPC-server ensuring communication between the PLC and LabView. In this configuration, the PLC and the LabView application are the OPC-clients. A LabView interface was also designed for human-machine interface. Moreover, LabView allows the interaction between the PLC and Matlab & Simulink software for simulation tests.

Figure 2 shows the automation structure of the process. This includes the human-machine interface at the top (LabView), the control part (PLC), sensors, drivers and the actuators at the bottom. With this layout, it is possible to measure and collect data from the system and manipulate the various actuators.

A command board was designed and assembled to keep the equipment safe, to protect the laboratory power network and for possible separate interruption of the reactors.

2.3. Data Logging

The data logging has two structures: (i) OPC connection between the LabView application and the PLC that records the data from the process every second; (ii) data logging that records data every 5 mins. The data files can be downloaded by accessing the PLC memory via a web-browser using the PLC address in the network (The PLC has 15 days of autonomy).

Before any data acquisition and process operation, instrument calibration was executed. An optical densitometer was used to measure the total suspended solids (TSS) concentration. It was calibrated by taking samples from the pipe between the denitrification and nitrification tanks, from the nitrification tank and a dilution of 1:2 from the latter. The samples were dried in an oven set to 105 ℃ and then the dry solid particles were weighed. The relation between measurements was computed by a linear regression method and is described using the following equation: X[g/L] = 1.6245·[CU]-0.009 with R^2 = 0.9996, where CU is the measurement provided by the optical densitometer.

A PT-100 sensor was added into the sMBR to measure the bulk temperature. The conversion of the PLC values to temperature is T_b[℃] = 0.008·T_{PT100}-12.31 with R^2 = 0.9993, where T_{PT100} represents values measured by the PLC.

PI controllers are used in the basic automation layer, in order to control the pump flow rates using the signals from the flow-meters.

3. Parameter Identification of a Simple Dynamic Model

The development of dynamic models linking the biological degradation and the filtration mechanism is extremely important to understand and optimize sMBR processes [20]. In recent years, many models with different complexities have been developed with the objective of understanding and monitoring the process dynamics [21, 22, 23, 24]. In a RAS, the recirculation increases the complexity of the process dynamics, making the system surprisingly difficult to operate and to maintain in the desired operating zone.

To alleviate this difficulty, model-based control is an appealing solution, and a simple dynamic model has been proposed in [14]. For the sake of conciseness, the model derivation is not repeated here, but attention is focused on the resulting set of ordinary differential equations and their interpretation. This model, which involves 4 state variables and 10 parameters, is given as follows:

$$\begin{cases} \dfrac{d\beta}{dt} = \gamma\beta & \text{(1a)} \\ \dfrac{dM}{dt} = Q_{out}X - J_{air}\mu_{air}(M)M & \text{(1b)} \\ \dfrac{dS}{dt} = -\dfrac{1}{Y}\mu(S)X + \dfrac{Q_{in}}{V}(S_{in} - S) & \text{(1c)} \\ \dfrac{dX}{dt} = \left(\mu(S) - \dfrac{Q_w}{V}\right)X + \dfrac{Q_{in}}{V}X_{in} - \dfrac{Q_{out}}{V}X + \dfrac{J_{air}}{V}\mu_{air}(M)M & \text{(1d)} \end{cases}$$

The notations are summarized in Table 1 and Figure 3 shows a simplified representation of the aerobic zone in a RAS process.

The first two equations describe membrane fouling, whereas the last two represent biological degradation. More specifically, the reversible layer dynamic in Eq. (1b) is described by two terms. The first term represents the attachment of suspended particles on the membrane surface, which is proportional to the effluent flow rate Q_{out} and suspended solid bulk concentration X. The second term represents the layer detachment, which is proportional to air cross-flow J_{air}, and

$$\mu_{air}(M) = \beta\frac{M}{K_{air} + M} \tag{2}$$

where M is the layer mass and K_{air} [g] is a half-saturation coefficient. The time-varying parameter β is a key factor of the model and represents the capacity of detaching the reversible cake layer from the membrane by air scouring (air cross-flow J_{air}). Considering a process with constant permeate flow ($Q_{out} \approx constant$), the capacity of the air cross-flow J_{air} to detach the reversible layer decreases with time due to the drag force on the solid particles. This is modeled as a decay of β, and a negative parameter γ [d^{-1}] in Eq. (1a) (with a small absolute value as the time evolution is quite slow as evidenced in experimental studies).

The biological activity is described as in the classical chemostat model [25], involving one hypothetical microbial biomass growing on a limiting substrate.

Equation (1c) represents the consumption of the substrate by the free biomass,

according to a Monod law

$$\mu(S) = \mu_{S,max} \frac{S}{K_S + S}, \tag{3}$$

and a biomass yield coefficient Y [−], where $\mu_{S,max}$ [d^{-1}] is the the maximum specific growth rate of the free biomass, K_S [g/m^3] is the half-saturation coefficient. Equation (1c) also includes transportation of inflowing and outflowing substrate through the tank.

In Equation (1d), material transportation involves waste flow, inflow and outflow, as well as the "conversion" of attached biomass into suspended solids due to the air cross-flow J_{air}/V $\mu_{air}(M)M$.

Usually, the reversible layer mass cannot be measured due to the lack of reliable sensors [26]. Thus, the trans-membrane pressure is used to control the sludge cake mass build-up indirectly, according to the following equation:

$$TMP = \frac{Q_{out}}{A} \eta R_{total} \tag{4}$$

where $R_{total} = R_m + R_{irr} + R_{rev}$ [m^{-1}] is the total fouling resistance, Q_{out} is the permeate pump flow selected by the operator (or the controller) and η [mbar d] is the apparent bulk viscosity, which can be modeled by [27]:

$$\eta(T_b) = A_1 e^{\frac{A_2}{T_b}}, \tag{5}$$

where T_b is the bulk temperature and A_1 and A_2 are apparent viscosity parameters.

The total resistance includes the reversible resistance R_{rev} due to the sludge cake described by

$$R_{rev} = \rho_{rev} \frac{M + M_0}{A}, \tag{6}$$

where ρ_{rev} [m/g] is the specific reversible resistance, M_0 [g] is the initial fouling mass, M [g] is the reversible fouling mass and A [m^2] is the membrane area.

The model derived in [14] was initially validated by comparison with a more complex biological and filtration model for wastewater treatment as implemented in the environment GPS-X [28]. In this work, experimental data will now be used for the model identification and validation.

3.1. Model Parameter Identification

The objective of parameter identification is to infer a set of parameters from experimental data, such that the proposed dynamic model can mimic the process behavior with satisfactory accuracy. The procedure is based on the minimization of a cost function that measures the deviation between experimental data and model outputs. In this study, the following weighted least-squares cost function

$$J(\theta) = \sum_{i=1}^{n_t} \left((\xi_{sim}(i) - \xi_{pilot}(i)) \right)^T \Xi^{-1} \left((\xi_{sim}(i) - \xi_{pilot}(i)) \right) \tag{7}$$

is minimized, where $\xi_{pilot} = [S_{pilot}\ X_{pilot}\ TMP_{pilot}]^T$ is the vector of measured variables and $\xi_{sim}(\theta) = [S_{sim}(\theta)\ X_{sim}(\theta)\ TMP_{sim}(\theta)]^T$ is the vector of simulated variables depending on the parameter set $\theta = [\beta_0,\ K_{air},\ \rho_{rev},\ M_0,\ Y,\ \mu_S,\ K_{air},\ \gamma,\ A1,\ A2,\ \rho_{irr}]$, n_t is the number of measurements and Ξ is defined as a scaling matrix that is selected as a diagonal matrix of the square of the maximum values corresponding to each state. The superscript ^{T} denotes the matrix transpose. The optimization is performed in this study using the Nelder-Mead algorithm as implemented by the *fminsearch* function in Matlab.

A lower bound of the covariance matrix $\hat{P}$ of the estimated parameters is obtained by the inverse of the Fisher Information Matrix (FIM):

$$\hat{P} = F^{-1}(\hat{\theta}, \Omega) \tag{8}$$

The FIM is computed by:

$$F(\hat{\theta}) = \sum_{i=1}^{n_t} \left[\frac{\partial Y_m}{\partial \theta} \right]^T_{(t_i, \hat{\theta})} \Omega^{-1} \left[\frac{\partial Y_m}{\partial \theta} \right] \tag{9}$$

where Y_m is the vector of the process outputs, Ω is the estimated covariance matrix

$$\Omega = \frac{J(\hat{\theta})}{(n_t - p)}\Xi \tag{10}$$

and p is the number of parameters to be estimated.

The square root σ_j of the j^{th} diagonal element of $\hat{P}$ is an estimate of the standard deviation of $\hat{\theta}_j$, which can be used to compute parameter confidence intervals. For instance, an interval of $\pm$ 1.96σ corresponds to a probability of 95%.

As the model analysis presented, [14] reveals, the sMBR process has three time-scales: the ultra-fast, fast and slow time-scales. This time-scale separation is exploited in the present study to simplify the identification procedure, which is organized in three steps, with each of the steps corresponding to one of the time-scales. A global identification of all the parameters simultaneously is, indeed, not a simple task and would lead to the occurrence of several local minima for the weighted least-square criterion that has been considered. A "divide-and-conquer" approach is therefore preferred, then one subset of parameters is estimated first, while another subset of parameters is estimated, with the first subset fixed. The procedure can be iterated, getting parameter values closer and closer to the sought optimum. If needed, a global identification can conclude this iterative procedure (in the global identification, all the parameters are freed, and the identification is initiated from the best values obtained in the "divide-and-conquer" procedure), the application of this procedure is presented in Section 4.3.

4. Results

The RAS-sMBR was operated over one year continuously with an input ammonia mass flow of 19.8 mg/h. Fresh water was only necessary to maintain the total volume of the process constant, in order to compensate for evaporation or technical problems. As a result, the total ammonia concentration in the process

was 0.177 ± 0.098 mg/L (considering 95% confidence intervals), which guarantees favorable environmental conditions for fish growth. Figure 4a compares a water sample from the sMBR tank with a water sample from the permeate flow. The efficiency of the membrane in terms of retention of solid matter is obvious. The high quality of the effluent is one of the most significant advantages of sMBR processes in a RAS. This high quality is not only linked to low turbidity, but also to the capacity of preventing fish diseases as a result of the retention of the disease agents in the extremely small pores of the membrane.

During the year of operation, different tests were executed and experimental data were analyzed in order to understand the process behavior. One of the experimental data sets was selected with the objective of identifying the parameters of the model presented in Section 3. Figure 5 shows experimental data recorded during one month. The trans-membrane pressure (TMP), which is linked to the fouling build-up, is visible in the first plot, and the constant effluent flow (Q_{out}), bulk temperature (T_b), total suspended solids (TSS), pH and air cross-flow (J_{air}) can be observed in the other plots. In the plot of NH_4^+, the ammonia values fluctuate as a result of the operating conditions used to obtain informative data for the dynamic response of the biological process, which are detailed in Section 4.3.

In order to understand specific properties of the RAS-sMBR, experiments focusing on the filtration characteristics of the plant were carried out. The process had a low concentration of TSS (around 0.2 g/L) compared to conventional activated sludge processes for wastewater treatment. Consequently, not much fouling occurred,as shown by the fact that, after five months in use, TMP reached 200 mbar (considered in this work the maximum pressure value for the membrane). This observation is explained by the low concentration of ammonia (and no carbon sources) in the synthetic water added into the fish tank. It is important to highlight that fouling in a RAS is associated with the fish diet, which is an important point for future research. The surface of the membrane was inspected visually. Figure 4b shows the material attached to the membrane. After the membrane was mechanically cleaned with brushes, TMP

dropped from around 200 to 45 mbar.

4.1. Critical Flux

To study the filtration characteristics, the "critical flux" was determined. This involves varying the permeate flow in order to observe the TMP behavior. The critical flux is reached when the relation between the flux and the TMP is no longer linear. The step method proposed in [29] was implemented.

Using the PI controller, the permeate flow was changed stepwise, with amplitude of 8.14 L/m^2/h over five-minute periods Fig. 6. The test shows that, in the considered operating conditions, the critical flux was not reached. This occurred probably due to the low concentration of suspended solids (0.130 g/L). The reversible layer on the membrane surface was extremely thin, while the TMP increased because of irreversible sludge deposition. This shows that the scouring produced by the air cross-flow is sufficient to control reversible sludge cake deposition, and the irreversible fouling is the main process in the TMP build-up.

Note that when the permeate flow is decreased, the TMP does not follow the same profile as Q_{out}. This can be explained by the air trapped inside the membrane structure, which affects the TMP profile. Relaxation with air purge cycles must be done to prevent accumulation of air in the membrane.

4.2. Air Cross-Flow Study

Over approximately 15 days, two experiments were set up for the study of fouling evolution. Air cross-flows with $J_{air} = 22.85$ m^3/m^2/d and $J_{air} = 53.85$ m^3/m^2/d were selected, respectively. For evaluating the fouling evolution slope, a second order low pass Butterworth-filter, Eq. (11), with a cut-off frequency of $\omega_c = 0.0209$ rad/s was designed, considering the permeate and relaxation cycles (5:1 min):

$$|B(j\omega)|^2 = \frac{1}{1 + (j\omega/j\omega_c)^{2N}} \tag{11}$$

Figure 7 shows the evolution of the TMP profiles in both experiments, which are quite similar. These tests show that reversible fouling was not present: changing the inlet air flow does not affect the profile slope in the long-term evolution. Thus, the TMP escalates due to the effect of the irreversible fouling layer on the membrane surface. This kind of observation could be used to reduce the air-cross flow to the minimum necessary (i.e., if two different air-cross flows result in the same TMP profiles, then the lower air flow is sufficient, and might even be further reduced upon further tests). This would contribute to a more profitable process, since the air blowers represent 80% of the total energy consumption of the sMBR process [9].

4.3. Model Identification and Cross-validation

The analysis of the process dynamics reveals that the process has three main time-scales: an ultra-fast, a fast and a slow time-scale [14]. This time-scale separation is used to segment the identification procedure into several smaller and easier to handle subproblems. The iterative procedure is represented in Figure 8. The data are therefore observed in time windows of different sizes, according to the time-scale separation, and according to their information content. It is important to note that data sets with enough information content must be selected to ensure parameter identifiability. At each step, the iterative procedure uses the previous best estimates. Also, a final global identification can be achieved, where all the parameters are estimated at once.

The attachment of the reversible layer is considered as an ultra-fast process and its parameters $\theta_{UF} = [K_{air}, \rho, M_0]$ are identified using a one-hour data set of measurements. The biological degradation and growth are considered as fast processes and their parameters $\theta_F = [Y, \mu_S, K_S]$ are identified using a three-day data set. The slow dynamic depends on the long-term fouling evolution, the irreversible resistance mechanism and the influence of the temperature on the apparent viscosity. The set of parameters $\theta_S = [\gamma, A1, A2, \rho_{irr}]$ is identified using a 16-day data set.

The procedure uses initial parameter values inspired by physical interpreta-

tion, literature study and knowledge about the process dynamic behavior. For example, the parameters ρ and M_0 influence the TMP initial amplitude, K_{air} influences the detachment by J_{air}, and γ and ρ_{irr} are linked to the TMP slope. Before starting the identification procedure, the data set is analyzed and a data window is selected such that it includes the required input and output signals, namely Q_{out}, J_{air}, X and T_b as inputs and TMP as output, with ideally no data acquisition interruptions.

Ultra-fast Dynamics Identification:. The ultra-fast dynamics are linked to the attachment and detachment of reversible sludge, which influence the TMP. Over this time-scale, neither the biological degradation nor the long-term fouling evolution are taken into account; they are considered constant due to their slow dynamic behavior (see the first column of Figure 8). The parameter identification procedure is used with a one-hour data period to identify K_{air}, ρ and M_0. Figure 9 shows that the dynamic behavior of TMP measurements (in green dashed line) is slower than the predictions of the proposed model (in dark blue line). This discrepancy is linked to the fact that the model does not take the air compression inside the tubes of the pilot plant into account. For the identification procedure, this drawback can be overcome using the average values of the TMP amplitude from each cycle.

Table 2 presents the identified parameter values with their 95% confidence intervals. The second column of this table shows the identified parameter values found by minimizing the cost function Eq. (7) considering the ultra-fast parameters and the one-hour experimental data set. The small value found for M_0 is in agreement with the small quantity of sludge observed in the real process. The identification result has a coefficient of determination $R^2 = 0.8813$. Note that the initial condition of β, β_0, could not be identified with this set of experimental data, thus the parameter was fixed at 55000 m^{-1}, as in [14]. A future investigation to find an appropriate set of experimental data for identification of this parameter should be carried out.

Fast Dynamics Identification:. Ammonia degradation and biomass growth can be considered as fast dynamics. As the process operates in a stationary regime, with constant ammonia inflow, disturbances were added to the ammonia inflow to extract information about the biological degradation dynamics (see the disturbances in the ammonia plot in Figure 5 after day 27). The disturbances were created by adding 0.1 L of a solution with 850 mg/L of ammonia.

The identification of the parameters linked to the fast time-scale is carried out on the basis of the values estimated in the previous step regarding the ultra-fast time-scale. The initial concentrations of ammonia and biomass are measured $S_0 = 0.13$ mg/L and $X_0 = 0.25$ g/L and are not re-estimated at this stage. It is important to note that initial conditions for the several state variables can be considered as either known (measured with sufficient accuracy) or unknown. In the latter case, they can be identified (as was the case for M_0 in the previous step) or fixed when not enough information is contained in the experimental data (as was the case for β_0 in the previous step). The parameters Y, $\mu_{S,max}$ and K_{air} were identified over approximately 3.5 days and their values are presented in the third column of Table 2. Figure 10 shows the simulation results, which have coefficients of determination of $R^2 = 0.9026$ and $R^2 = 0.9745$ for TSS and ammonia concentration, respectively.

Slow Dynamics Identification:. The slow dynamics are linked to the long-term fouling evolution, which is expressed using the irreversible sludge layer, the long-term sludge cake evolution and the apparent viscosity parameters, which are the parameters ρ_{irr}, γ, A_1 and A_2, respectively. The long-term identification procedure uses a large data set covering 16 days (see Figure 11). The average value of the TMP over each cycle is computed and used in the identification procedure. The estimated parameter values and confidence intervals are shown in Table 2. The coefficient of determination of the model prediction is $R^2 = 0.8763$. The identified small value of γ, which is linked to the reversible sludge layer, shows that the main mechanism of fouling in RAS-sMBR is irreversible fouling.

The prediction of the long-term evolution is extremely important for the RAS-sMBR to be profitable. This prediction will help in scheduling the preventive maintenance of the process, and avoiding unexpected interruption of operation, which could severely damage fish production (through death due to high ammonia concentrations) and process profitability, due to the increase of the ratio between clean and reused water.

Note that the three time-scale identification procedure (Section 3.1) can be completed by a global identification, where all the parameters are estimated simultaneously, starting from the best values found in the separate steps. These procedures were implemented and no significant variation in the parameters, nor in the cost function value were observed, validating the three time-scale identification procedure.

Cross-validation:. Cross-validation was performed using experimental data that were not used in the identification procedure. The cross-validation of the ultra-fast dynamics is presented in Figure 12. The model with the identified parameters still can predict the attachment and detachment of sludge cake. Note that, over time, an undesirable amount of air inside the membrane structure accumulates, damping more and more the dynamic evolution of the TMP.

Figure 13 shows the cross-validation results linked to the biological degradation (fast-dynamics). In the cross-validation procedure different concentrations of ammonia and suspended solids are considered in order to test the domain of the validity of the identified parameters of the model. Note that the model still provides good prediction, which shows the large domain of validity of the model parameters.

The cross-validations of the slow dynamics are presented in Figure 14; the figures at the bottom show the simulation in more detail. A fair coefficient of determination is achieved ($R^2 = 0.8493$), showing the possibility to use the model as a predictor in long-term experiments.

5. Discussion

The main result of the previous section is to show that a simple dynamic model, with only 4 state variables, is able to capture the main dynamics of the wastewater treatment process. The identified parameter values are comparable to values reported in previous studies, such as: $\mu_{S,max} = 0.8$ d^{-1}, $K_S = 1.0$ g/m^3, $Y = 0.24$ in the study of a general model for wastewater treatment by [30]; $\mu_{S,max} =$ [0.7 - 0.8] d^{-1}, $K_S =$ [0.2 - 0.4] g/m^3 and $Y =$ [0.084 - 0.142] in the study of biofilters used for nitrification reported by [31], and $\mu_{S,max} =$ [0.74 - 1.47] d^{-1} when [32] analyzed the pH dependence of the maximum specific nitrification rate.

The model is grey-box in nature, since it neglects many phenomena, so as to keep a simple structure and a modest size (which would make it black box), while keeping the essential physical/biological structural elements, so as to fit the observed data with a small set of parameters. This is in contrast with true black-box models, which involve more parameters and usually require larger sets of data for their calibration. An associated advantage of this approach is that the model is interpretable, and could be accepted by practitioners if used within a model-based control strategy.

Another important observation of this study is that the biological dynamics of the RAS fitted with a sMBR are comparable to those of an ordinary nitrification process, and a relatively limited number of measurements is required to achieve a satisfactory identification based on the proposed 'divide-and-conquer' strategy, which therefore appears feasible in practice. Moreover, the procedure also requires less computational effort as compared to the identification of all the parameters simultaneously, as it uses a smaller time window. This aspect is important as identification is a time-consuming task, which might prevent practitioners from developing models of their plants.

Finally, the cross-validation tests (carried out with independent data sets) show that the model structure and the identified parameters capture the main process dynamics, over a range of operating conditions. The resulting simulator

could be used for prediction and monitoring.

6. Conclusions

In order to investigate recirculating aquaculture systems complemented with membrane bioreactors, a laboratory-scale system was designed and automated. This system allows experiments to be carried out over a large range of situations and the collected data can be used for the development of dynamic models. In particular, a simple dynamic model with 4 state variables and 10 parameters was identified and cross-validated with the data at hand. To this end, a dedicated identification procedure is proposed, which proceeds in three steps. It is to be stressed that this identification decomposition relies on the choice of three distinct time windows to operate the three identification steps in sequence. These windows are chosen based on an analysis of the three-scale model, and slow-fast approximations. Moreover, a cross-validation demonstrates the model adequacy, even outside the operating range used in the identification procedure. The resulting model could be used as a predictor in various model-based monitoring or advanced control strategies.

7. Acknowledgments

The authors acknowledge the support of the Walloon Region and the Wagralim Pole in the framework of the Nutrivert Project. This paper presents research results of the Belgian Network DYSCO (Dynamical Systems, Control, and Optimization), funded by the Interuniversity Attraction Poles Programme, initiated by the Belgian State, Science Policy Office. The scientific responsibility lies with its authors. The first author also thanks Dr. Jérôme Harmand for valuable advice in this project. The authors are grateful to UMONS (Belgium), to INRA (France), to CAPES and CNPq (Brazil) for the co-funding of the first author.

References

[1] R. H. Piedrahita, Reducing the potential environmental impact of tank aquaculture effluents through intensification and recirculation, Aquaculture 226 (2003) 35–44.

[2] W. Hutchinson, M. Jeffrey, D. D. O'Sullivan, D. Casement, S. Clarke, Recirculating aquaculture systems: minimum standards for design, construction and management., Kent Town, S. Aust. : Inland Aquaculture Association of South Australia, 2004.

[3] R. Crab, Y. Avnimelech, T. Defoirdt, P. Bossier, W. Verstraete, Nitrogen removal techniques in aquaculture for a sustainable production, Aquaculture 270 (2007) 1–14.

[4] K. Atasi, G. Crawford, J. M. Hudkins, D. Livingston, R. Reardon, H. Schmidt, Membrane systems for wastewater treatment, WEF Press, 2006.

[5] N. Cicek, A review of membrane bioreactors and their potential application in the treatment of agriculture wastewater, Canadian Biosystems Engineering 45 (2003) 6.37 – 6.49.

[6] G. D. Bella, G. Mannina, G. Viviani, An integrated model for physical-biological wastewater organic removal in a submerged membrane bioreactor: model development and parameter estimation, Journal of Membrane Science 322 (2008) 1–12.

[7] M. Sarioglu, G. Insel, N. Artan, D. Orhon, Model evaluation of simultaneous nitrification and denitrification in membrane bioreactor operated without an anoxic reactor, Journal of Membrane Science 337 (2009) 17–27.

[8] T. Nittami, H. Ootake, Y. Imai, Y. Hosokai, A. Takada, K. Matsumoto, Partial nitrification in a continuous pre-denitrification submerged membrane bioreactor and its nitrifying bacterial activity and community dynamics, Biochemical Engineering Journal 55 (2011) 101 – 107.

[9] S. Judd, C. Judd, The MBR book - Principles and applications of membrane bioreactors in water and wastewater treatment, 2nd Edition, Elsevier, 2011.

[10] A. Zarragoitia-González, S. Schetrite, M. Alliet-Gaubert, U. J. Haza, C. Albasi, Modelling of submerged membrane bioreactor: conceptual study about link between activated sludge biokinetics, aeration and fouling process, Journal of Membrane Science 325 (2008) 612 – 624.

[11] B. Gemende, A. Gerbeth, N. Pausch, A. von Bresinsky, Tests for application of membrane technology in a new method for intensive aquaculture, Desalination 224 (2008) 57 – 63.

[12] R. C. Viadero Jr., J. A. Noblet, Membrane filtration for removal of fine solid from aquaculture process water, Aquacultural Engineering 26 (2002) 151 – 169.

[13] T. Pulefou, V. Jegatheesan, C. Steicker, S.-H. Kim, Applications of submerged membrane bioreactor for aquaculture effluent reuse, Desalination 221 (2008) 534 – 542.

[14] G. A. Pimentel, A. Vande Wouwer, J. Harmand, A. Rapaport, Design, analysis and validation of a simple dynamic model of a submerged membrane bioreactor, Water Research 70 (2015) 97 – 108.

[15] G. A. Pimentel, A. Vande Wouwer, A. Rapaport, J. Harmand, Modeling of submerged membrane bioreactors with a view to control, in: 11th IWA conference on Instrumentation Control and Automation, 2013.

[16] E. Eding, A. Kamstra, J. Verreth, E. Huisman, A. Klapwijk, Design and operation of nitrifying trickling filters in recirculating aquaculture: A review, Aquacultural Engineering 34 (3) (2006) 234 – 260.

[17] S. L. Thomas, R. H. Piedrahita, Apparent ammonia-nitrogen production rates of white sturgeon (acipenser transmontanus) in commercial aquaculture systems, Aquacultural Engineering 17 (1998) 45–55.

[18] A. Gershanovich, I. Pototskij, The peculiarities of nitrogen excretion in sturgeons (Acipenser Ruthenus) (Pisces, Acipenseridae) - I. the influence of ration size, Comparative Biochemistry and Physiology Part A: Physiology 103 (3) (1992) 609–612.

[19] MICRODYN-NADIR GmbH - Advanced separation technologies, BIO-CEL: submerged modules for membrane bioreactors (2011).
URL http://www.microdyn-nadir.com/en/products/bio-cel/

[20] W. Naessens, T. Maere, N. Ratkovich, S.Vedantam, I. Nopens, Critical review of membrane bioreactor models - part 2: hydrodynamic and integrated models, Bioresource Technology 122 (2012) 107 – 118.

[21] X. Li, X. Wang, Modelling of membrane fouling in a submerged membrane bioreactor, Journal of Membrane Science 278 (1-2) (2006) 151 – 161.

[22] G. Mannina, G. Di Bella, V. G., An integrated model for biological and physical process simulation in membrane bioreactor (MBRs), Journal of Membrane Science 376 (2011) 56–69.

[23] A. Robles, M. Ruano, J. Ribes, A. Seco, J. Ferrer, A filtration model applied to submerged anaerobic MBRs (SAnMBRs), Journal of Membrane Science 444 (2013) 139 – 147.

[24] J. Busch, A. Cruse, W. Marquardt, Modeling submerged hollow-fiber membrane filtration for wastewater treatment, Journal of Membrane Science 288 (2007) 94 – 111.

[25] H. L. Smith, P. Waltman, The theory of the chemostat, Cambridge University press, 1995.

[26] M. Dalmau, I. Rodriguez-Roda, E. Ayesa, J. Odriozola, L. Sancho, J. Comas, Development of a decision tree for the integrated operation of nutrient removal MBRs based on simulation studies and expert knowledge, Chemical Engineering Journal 217 (2013) 174 – 184.

[27] F. A. Rodríguez, M. Martínez-Toledo, J. González-López, E. Hontoria, J. Poyatos, Performance of bench-scale membrane bioreactor under real work conditions using pure oxygen: viscosity and oxygen transfer analysis, Bioprocess and Biosystems Engineering 33 (2010) 885 – 892.

[28] Hydromantis - Environmental Software Solution, Inc, GPS-X, version 6.2.0, Software (2012).
URL http://www.hydromantis.com/GPS-X.html

[29] P. Le-Clech, V. Chen, T. A. Fane, Fouling in membrane bioreactors used in wastewater treatment, Journal of Membrane Science 284 (2006) 17 – 53.

[30] M. Henze, C. Leslie Grandy Jr, W. Gujer, G. Marais, T. Matsuo, A general model for single-sludge wastewater treatment system, Water Research 21 (1987) 505 – 515.

[31] I. Queinnec, J.-C. Ochoa, E. Paul, A. V. Wouwer, Dynamic modelling of a biofilter used for nitrification of drinking water at low influent ammonia concentrations, in: International Symposium on Advanced Control of Chemical Processes, 2006.

[32] S. Park, W. Bae, J. Chung, S.-C. Baek, Empirical model of the pH dependence of the maximum specific nitrification rate, Process Biochemistry 42 (2007) 1671 – 1676.

FIGURE CAPTIONS

Fig. 1. Pilot Description: DP1 is the ammonia dosing pump, M1 and M2 are the mixers, NH4 is the point of ammonia measurement, N0, N1, N2 and N3 are the tank level sensors, MP1, MP2 and MP3 are the magnetic pumps, F1, F2, F3 and F4 are the liquid flow-meter sensors, T1 is the denitrification tank, T2 is the nitrification tank, DF1 is the air diffuser, A1 and A2 are the air flow-meters, O1 is the measuring point for oxygen, P1 and P2 are the pressure sensors, V1,V2 and V3 are the direction valves and SP1 is the suction pump.

Fig. 2. Layers of automation of the laboratory-scale process.

Fig. 3. Simplified representation of the submerged membrane bioreactor (sMBR).

Fig. 4. Visual analysis of the effluent and cake deposition on the membrane. (a) Left: permeate sample. Right: sMBR tank sample. (b)Fouling deposit onto membrane surface.

Fig. 5. Measurements from one experiment.

Fig. 6. Critical Flux test with five-minute stepwise changes in the effluent flow (amplitude of steps: 8.14 L/m^2/h).

Fig. 7. Influence of different air cross-flow values on the TMP. Dark blue: J_{air} = 53.85 m^3/m^2/d; green dashed line: J_{air} = 22.85 m^3/m^2/d.

Fig. 8. Three-step identification procedure. The columns represent the several steps according to a time-scale separation and the lines the parameters to be estimated. θ_{UF}, θ_F and θ_S are the set of parameters linked to the ultra-fast, fast and slow dynamics, respectively.

Fig. 9. TMP **short-term behavior and ultra-fast dynamics. Dark blue line: model prediction; green dashed line: online measurements.**

Fig. 10. Biological degradation identification (Fast Dynamics). Dark blue line: model prediction; green dots: experimental data.

Fig. 11. Results of slow dynamic identification. Dark blue line: model prediction; green dots: mean value of each cycle computed from the real data. (a) Results for 16 days. (b) Zoom In on the initial times. (c) Zoom In on the final times.

Fig. 12. Cross-validation of the ultra-fast dynamics. Red-dashed line: experimental data; blue line: model prediction.

Fig. 13. Cross-validation of the fast dynamics. Red dots: experimental data; blue line: model prediction.

Fig. 14. Cross-validation of the slow dynamics. (a) Results for 4 days. (b) Zoom In on the initial times. (c) Zoom In on the final times. Red dots: the experimental data; blue line: model prediction.

Table 1
Symbols and Notations.

Symbol	Description
A_1	apparent viscosity [-] (model parameter)
A_2	apparent viscosity [-] (model parameter)
β	resistance of detachable cake to air cross-flow [m^{-1}](state variable)
η	apparent viscosity [mbar d]
J_{air}	air cross-flow [$m^3/m^2/d$]
K_{air}	half saturation constant for airflow [g] (model parameter)
K_S	half saturation constant for substrate [g/m^3] (model parameter)
M	mass of reversible fouling [g] (state variable)
M_0	initial mass of reversible fouling attached to the membrane [g] (model parameter)
μ	specific growth rate [d^{-1}]
$\mu_{S,max}$	maximum specific growth rate [d^{-1}] (model parameter)
Q_{in}	inflow [m^3/d]
Q_{out}	permeate flow [m^3/d]
Q_w	waste flow [m^3/d]
R_{irr}	irreversible fouling resistance [m^{-1}]
R_m	intrinsic membrane resistance [m^{-1}]
R_{rev}	reversible fouling resistance [m^{-1}]
R_{total}	total fouling resistance [m^{-1}]
ρ_{irr}	specific pore fouling resistance [m^2] (model parameter)
ρ_{rev}	specific reversible resistance [m/g] (model parameter)
S	substrate concentration [g/m^3](state variable)
S_{in}	input substrate concentration [g/m^3]
T_b	bulk temperature [℃]
$t_{permeate}$	duration of the permeate cycle [d]
t_{relax}	duration of the relaxation cycle [d]
TMP	trans-membrane pressure [mbar]
V	tank volume [m^3]
Y	biomass yield [-] (model parameter)
X	solid matter concentration [g/L](state variable)

[-] denotes dimensionless.

Table 2
Identified parameters with 95% confidence limits.

Parameters	Ultra-Fast Procedure	Fast Procedure	Slow Procedure
K_{air} [g]	(48.6 ± 2.3)	48.6^*	48.6^*
ρ_{rev} [m/g]	$(2.93 \pm 0.17) \times 10^{11}$	$2.93 \times 10^{11*}$	$2.93 \times 10^{11*}$
M_0 [g]	$(9.51 \pm 0.13) \times 10^{-1}$	$9.51 \times 10^{-1*}$	$9.51 \times 10^{-1*}$
Y [-]	0.4^*	(0.23 ± 0.14)	0.23^*
$\mu_{S,max}$ [d^{-1}]	0.9^*	(0.91 ± 0.69)	0.91^*
K_S [g/m^3]	0.1^*	(0.09 ± 0.10)	0.09^*
γ [d^{-1}]	-0.1^*	-0.1^*	$-(1.63 \times 10^{-13} \pm 1.6 \times 10^{-5})$
A_1 [-]	1.1^*	1.1^*	$(9.13 \pm 0.02) \times 10^{-1}$
A_2 [-]	13.5^*	13.5^*	(7.84 ± 0.02)
ρ_{irrev} [m^{-2}]	$8.0 \times 10^{7*}$	$8.0 \times 10^{7*}$	$(8.33 \pm 0.02) \times 10^7$

*Constant value in this identification procedure

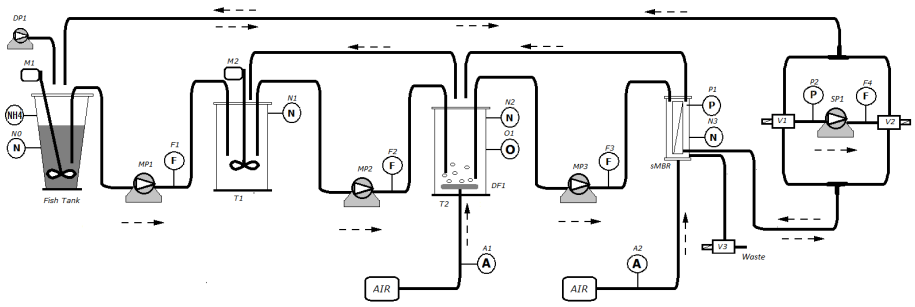
DP1
M1
NH4
NO
N
Fish Tank
MP1
F1
F
M2
T1
N1
N
MP2
F2
F
T2
N2
N
O1
O
DF1
A1
A
AIR
MP3
F3
F
sMBR
P1
P
N3
N
A2
A
AIR
V3
Waste
P2
P
SP1
F4
F
V1
V2

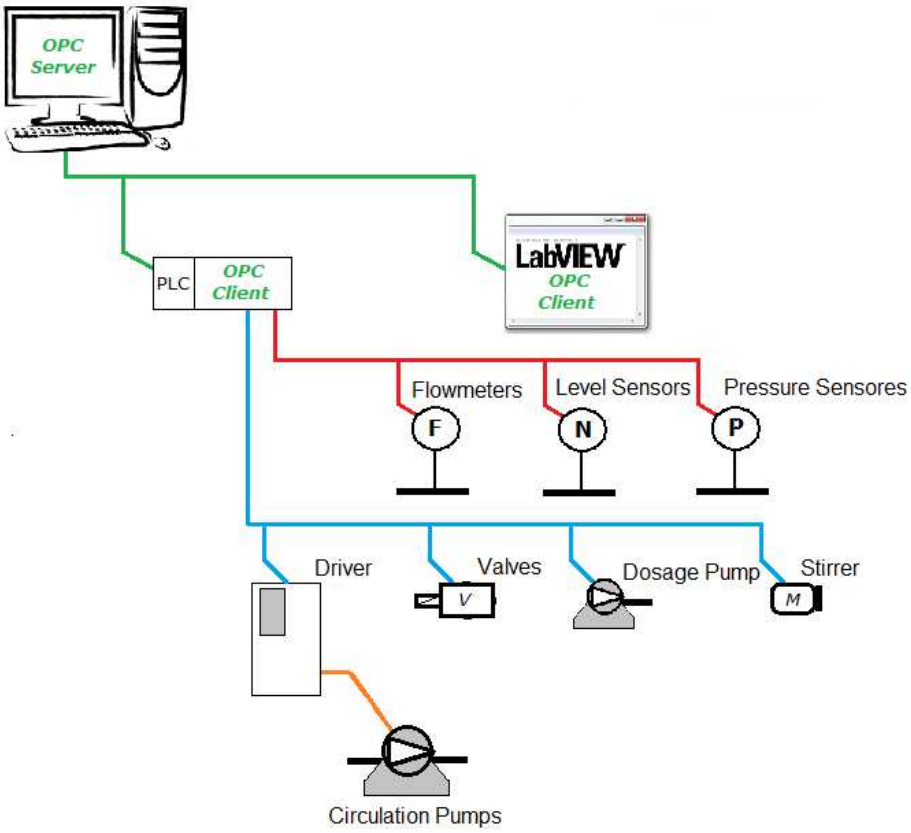
OPC
Server
PLC
OPC
Client
LabVIEW
OPC
Client
Flowmeters
Level Sensors
Pressure Sensores
F
N
P
Driver
Valves
V
Dosage Pump
Stirrer
M
Circulation Pumps

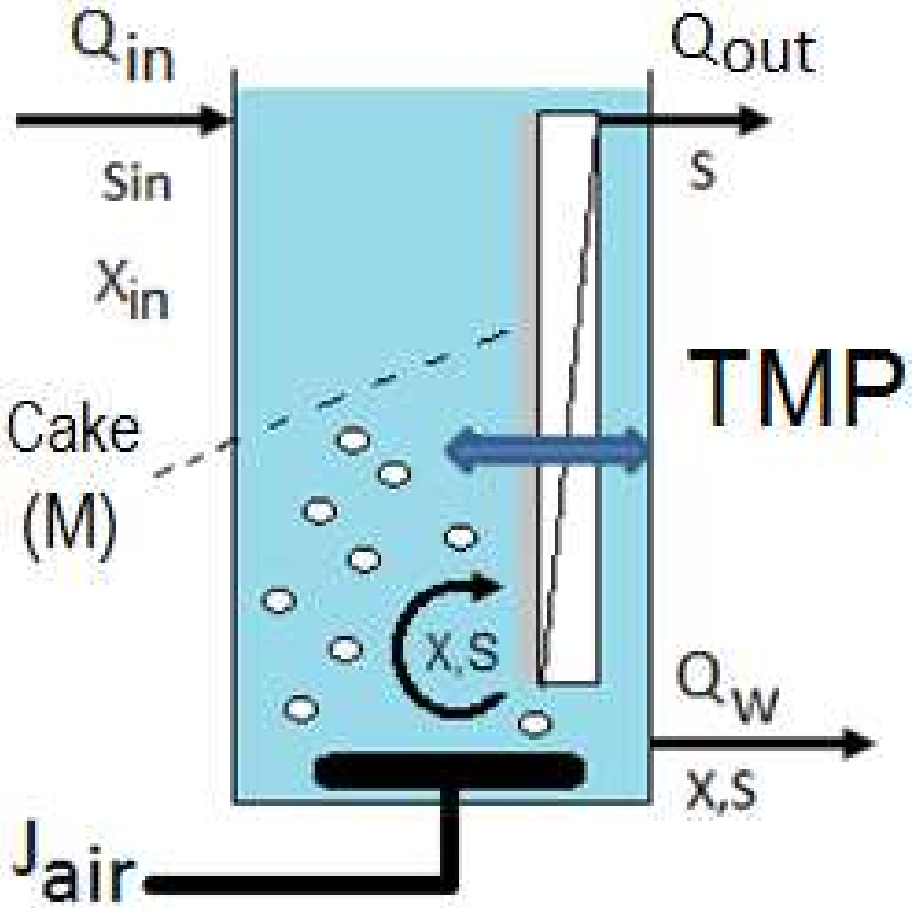
Q_{in}
Q_{out}
Sin
S
X_{in}
TMP
Cake
(M)
X,S
Q_w
X,S
J_{air}

(a)

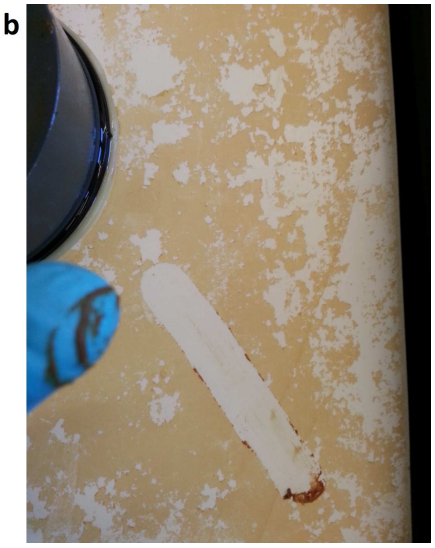

(b)

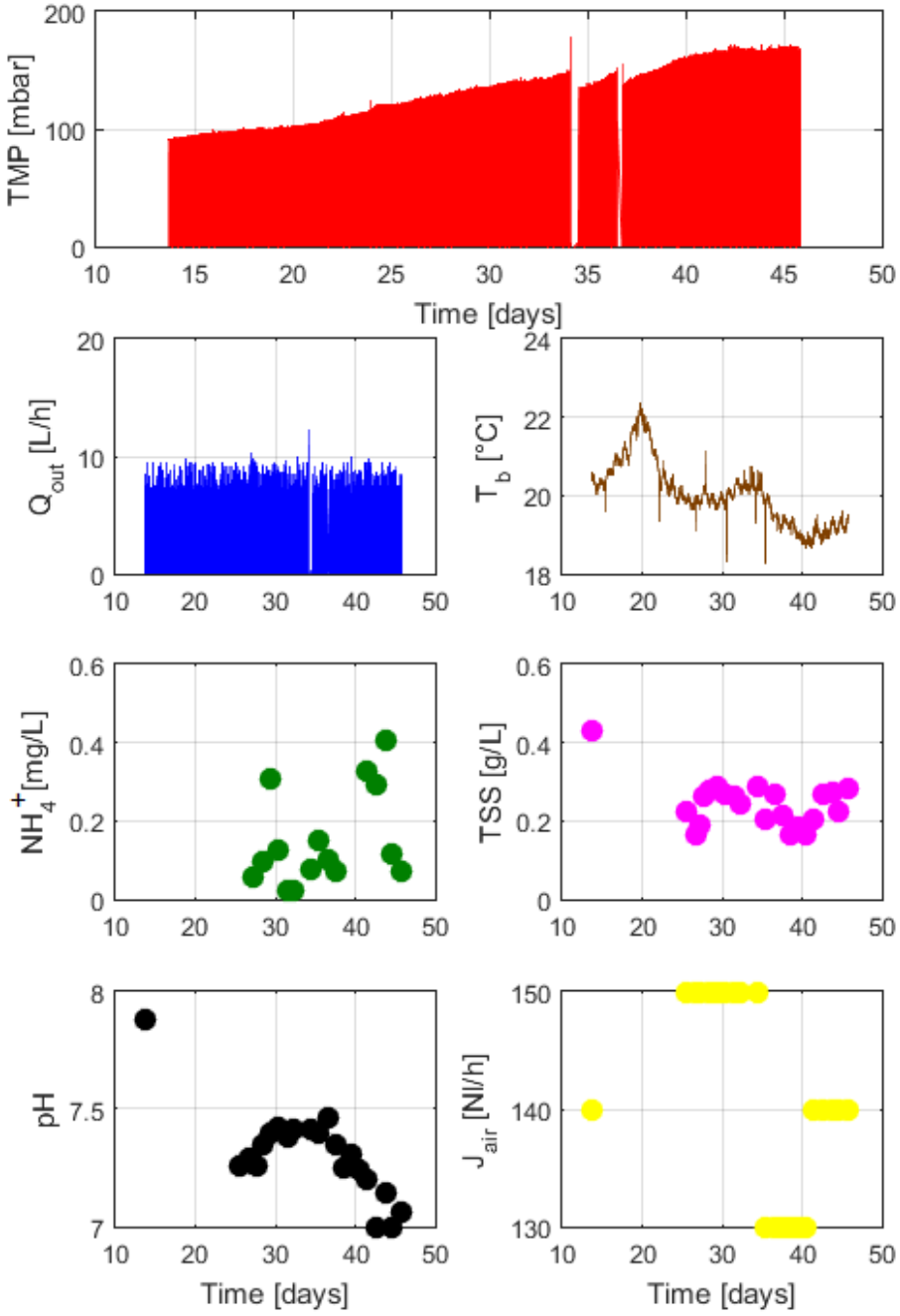
TMP [mbar]
Time [days]
Q_{out} [L/h]
T_b [°C]
NH_4^+[mg/L]
TSS [g/L]
pH
J_{air} [Nl/h]
Time [days]
Time [days]

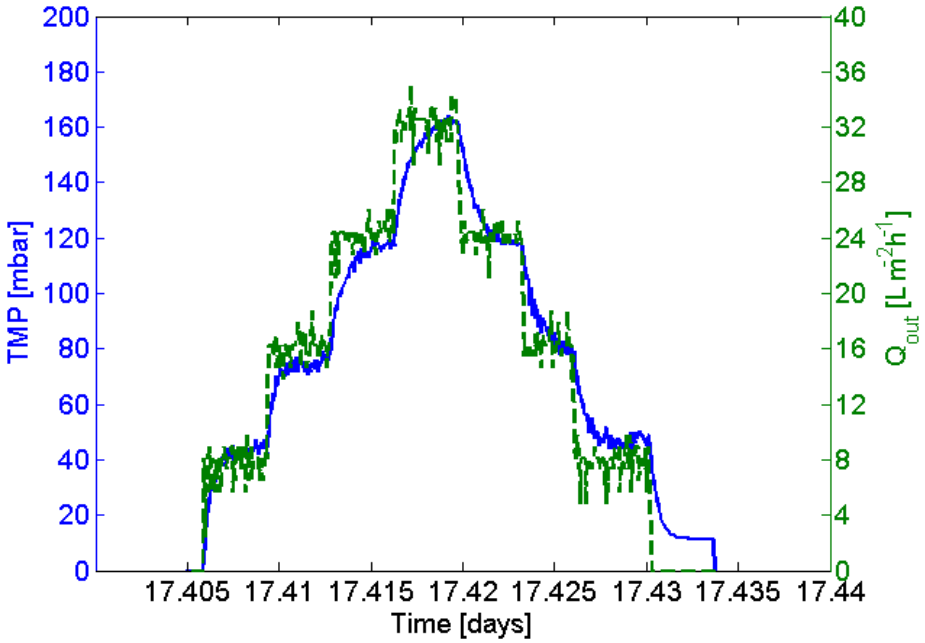
200
180
160
140
120
100
80
60
40
20
0
TMP [mbar]
40
36
32
28
24
20
16
12
8
4
0
Q_{out} [L m^{-2}h^{-1}]
17.405
17.41
17.415
17.42
17.425
17.43
17.435
17.44
Time [days]

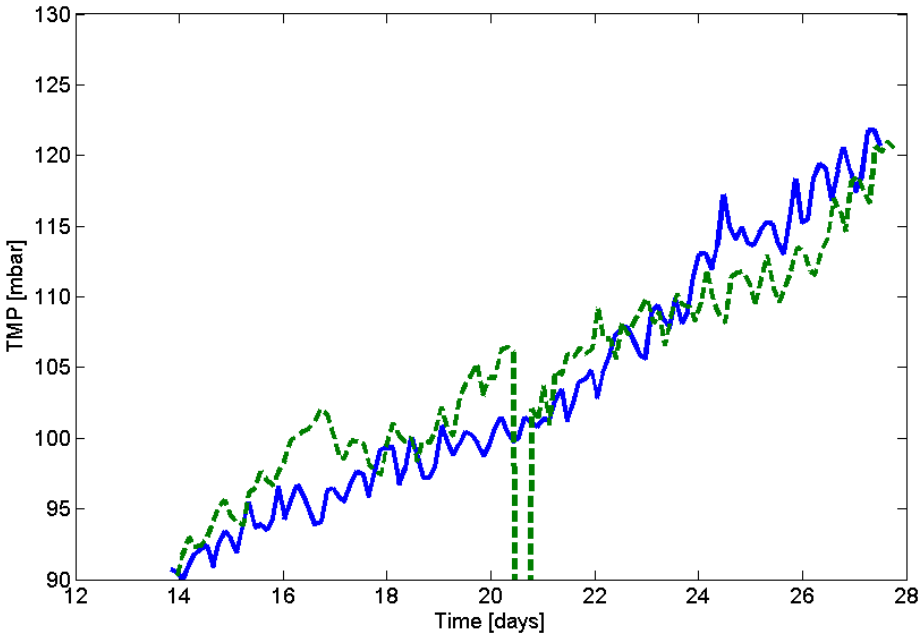
TMP [mbar]
Time [days]
130
125
120
115
110
105
100
95
90
12
14
16
18
20
22
24
26
28

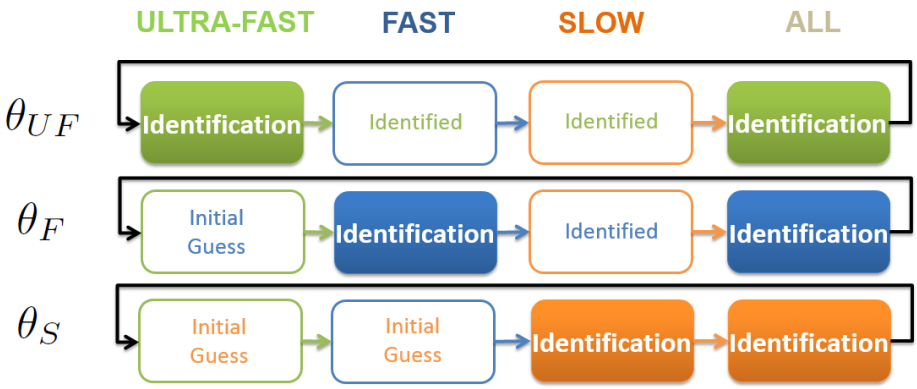
ULTRA-FAST
FAST
SLOW
ALL
θ_{UF}
Identification
Identified
Identified
Identification
θ_F
Initial Guess
Identification
Identified
Identification
θ_S
Initial Guess
Initial Guess
Identification
Identification

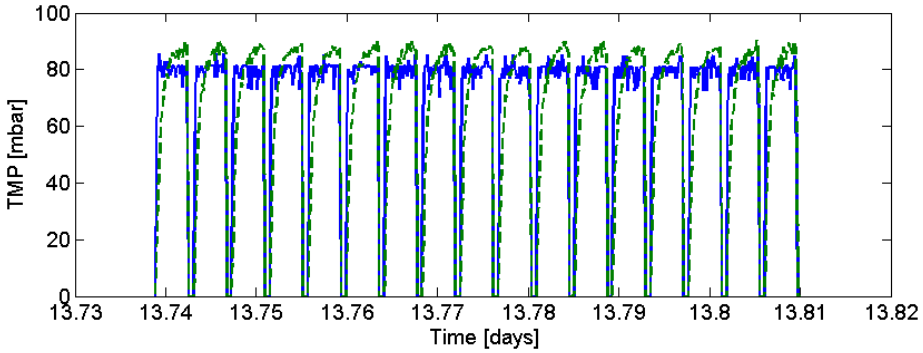
100
80
60
40
20
0
TMP [mbar]
13.73
13.74
13.75
13.76
13.77
13.78
13.79
13.8
13.81
13.82
Time [days]

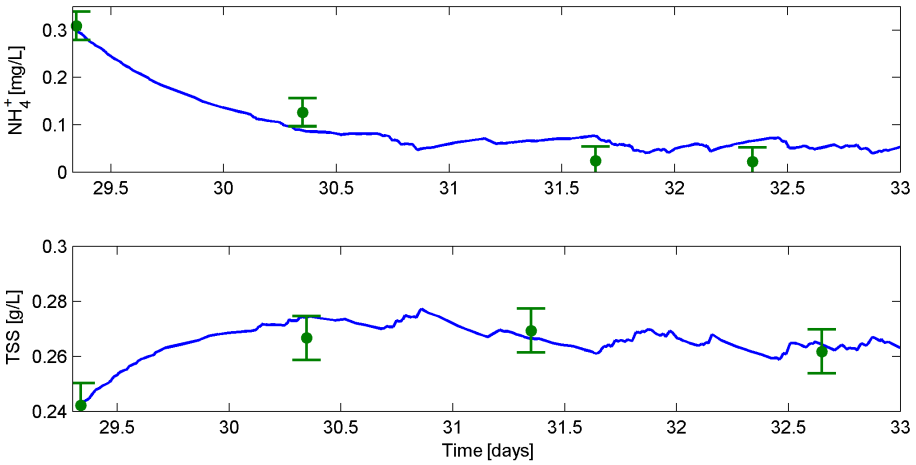
NH_4^+ [mg/L]
0.3
0.2
0.1
0
29.5
30
30.5
31
31.5
32
32.5
33
TSS [g/L]
0.3
0.28
0.26
0.24
29.5
30
30.5
31
31.5
32
32.5
33
Time [days]

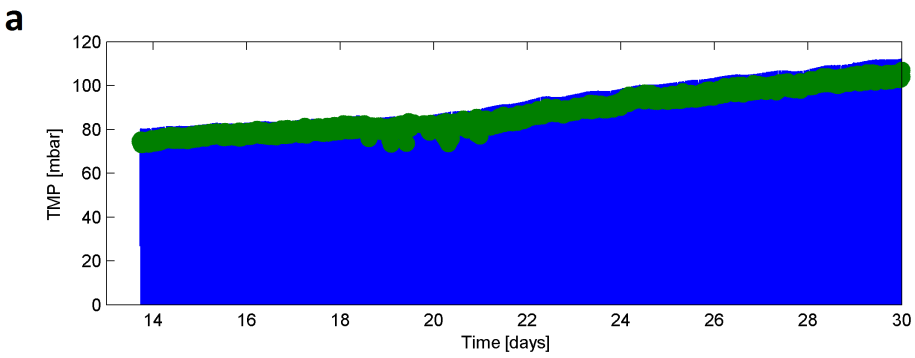
a
120
100
80
60
40
20
0
TMP [mbar]
14
16
18
20
22
24
26
28
30
Time [days]

(a)

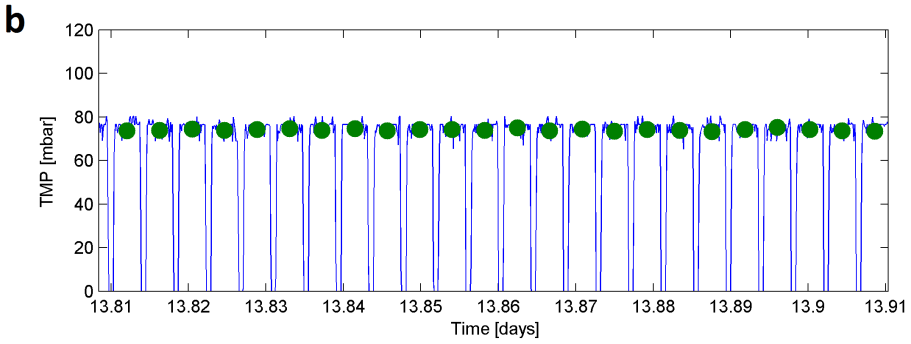
b
120
100
80
60
40
20
0
TMP [mbar]
13.81
13.82
13.83
13.84
13.85
13.86
13.87
13.88
13.89
13.9
13.91
Time [days]

(b)

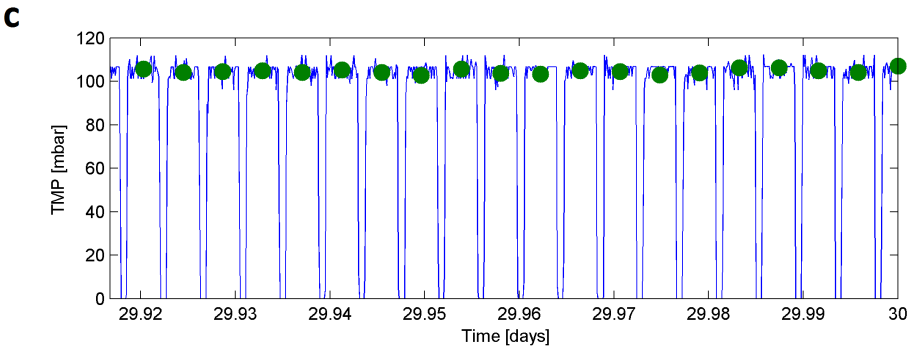
c
120
100
80
60
40
20
0
TMP [mbar]
29.92
29.93
29.94
29.95
29.96
29.97
29.98
29.99
30
Time [days]

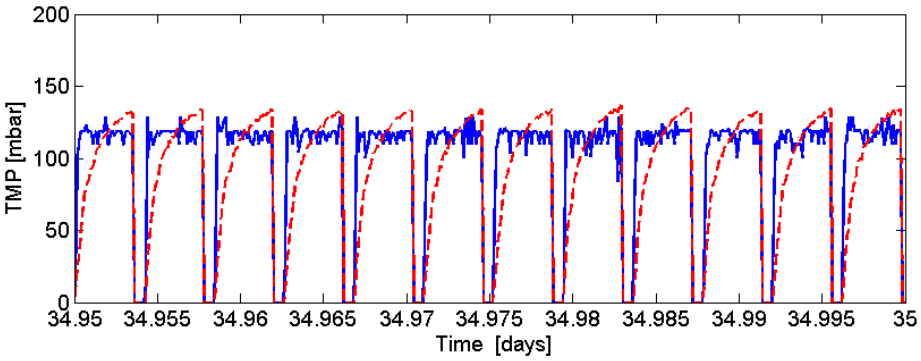
200
150
100
50
0
TMP [mbar]
34.95
34.955
34.96
34.965
34.97
34.975
34.98
34.985
34.99
34.995
35
Time [days]

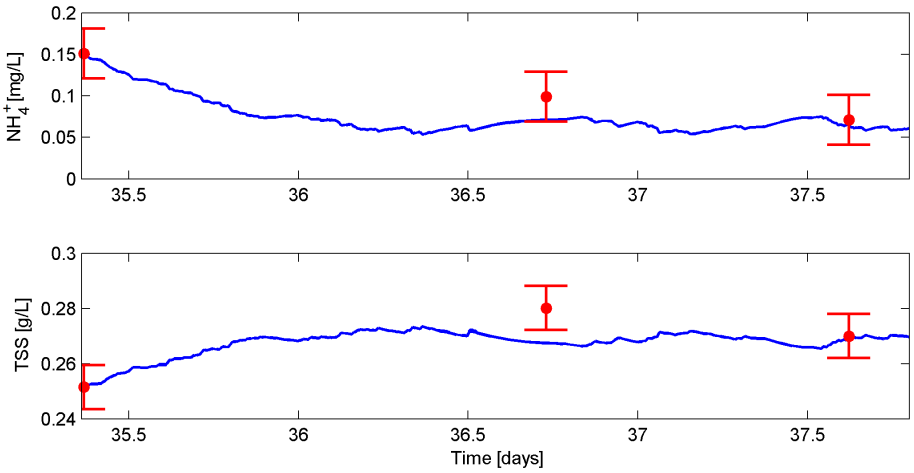
0.2
0.15
0.1
0.05
0
NH_4^+ [mg/L]
35.5
36
36.5
37
37.5
0.3
0.28
0.26
0.24
TSS [g/L]
35.5
36
36.5
37
37.5
Time [days]

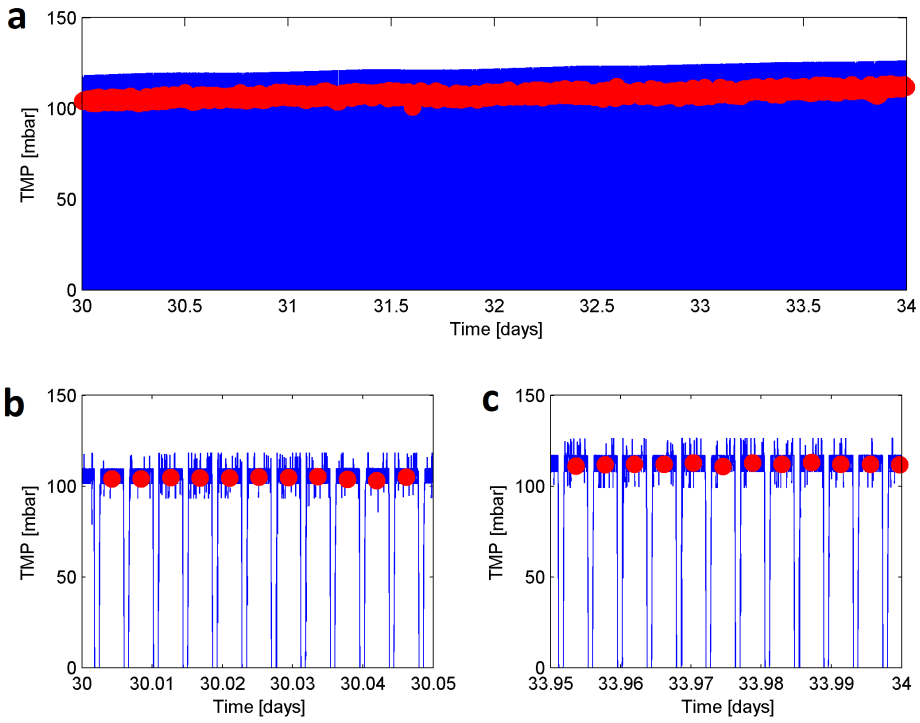
a
150
100
50
0
TMP [mbar]
30
30.5
31
31.5
32
32.5
33
33.5
34
Time [days]
b
150
100
50
0
TMP [mbar]
30
30.01
30.02
30.03
30.04
30.05
Time [days]
c
150
100
50
0
TMP [mbar]
33.95
33.96
33.97
33.98
33.99
34
Time [days]